Macromolecules

ARTICLE

pubs.acs.org/Macromolecules

Stress−Strain Behavior, Elastic Recovery, Fracture Points, and Time−Temperature Superposition of an OOT-Possessing Triblock Copolymer

Yoshinori Orimo and Atsushi Hotta*

Department of Mechanical Engineering, Keio University, Yokohama 223-8522, Japan

Supporting Information

ABSTRACT: The microphase-separated structures of block copolymers have been widely studied to understand the complex mechanism and the comprehensive framework of the microphase separation of the copolymers, which depended primarily upon the copolymer composition, the molecular weight, and temperature. In this work, the morphology and the mechanical properties of a SIS triblock copolymer with 18.3 wt % of polystyrene (Vector 4111) were investigated. Vector 4111 was structurally quite unique in the sense that it possessed two order−order transitions at different temperatures and an order−disorder transition at high temperature. The different microstructures in the different phases of Vector 4111 were obtained by annealing at different temperatures, confirmed by AFM and SAXS: the hexagonally aligned cylindrical phase was obtained when annealed below 185 °C, the spherical phase adopting a body-centered cubic (BCC) arrangement was formed at 185 °C < T < 215 °C, the misaligned spherical phase was obtained at 215 °C < T < 280 °C, and finally the completely disordered phase was obtained above 280 °C. The mechanical testing of Vector 4111 in the different phases was conducted by measuring the stress−strain behavior, the fracture points, the elastic recovery rates, and the elastic modulus followed by the evaluation of the time−temperature superposition. From the results of the stress−strain measurements, it was found that both elastic modulus and fracture stress of the sample in the cylindrical phase were highest, getting lower in the order of BCC spherical, misaligned spherical, and disordered phases, examined by a universal testing machine. It was also found that the time−temperature superposition was valid only within the same microphase-separated region or within the disordered phase. This study would provide an overall picture regarding the relationship between the microstructures and the mechanical properties, including the nonlinear mechanical properties, of a triblock copolymer possessing order−order transitions (OOT) and an order−disorder transition (ODT).

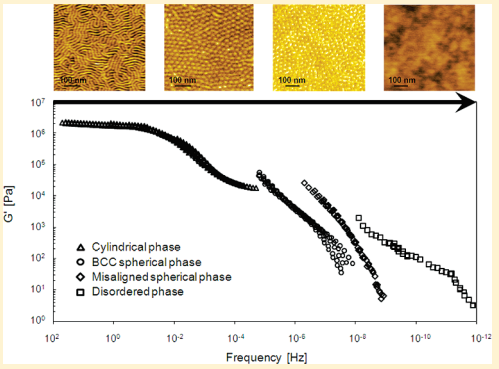

INTRODUCTION

Triblock copolymers have been widely investigated because they possess both elastomeric and thermoplastic features due to its microphase-separated structures.[1−3] Figure 1 shows the phase diagram of microphase-separated structures as functions of the molecular composition f, the segment−segment interaction energy χ (the Flory−Huggins interaction parameter), and the degree of polymerization N,[4−6] where χ is known to be inversely proportional to the temperature T.[7,8] Changing the composition from 0 to 1, the morphology of the triblock copolymer would generally transform from spheres, through cylinders, into lamellas, followed by the phase inversion process of the structural transitions. Such phase transitions can be practically traced by producing different compositions of copolymers as the change in the positive direction of the x-axis in Figure 1.[9−11] Since χN (y-axis) is also directly related to the degree of polymerization and temperature, such phase transitions could also be detected by changing N and T as the change in y-axis in Figure 1. The phase transition of block copolymers appears as an order−order transition (OOT) where an ordered structure transforms to the other ordered structure, or it appears as an order−disorder transition (ODT) where an ordered structure transforms into a disordered structure.[12,13]

The relationship between the mechanical properties and the phase behaviors of block copolymers has been intensely investigated through the analysis of the microstructures of the block copolymers with different compositions by the x-axis change (Figure 1).[14,15] For example, Honeker et al. controlled the morphology of polystyrene (PS)−polyisoprene (PI)−polystyrene (SIS) by changing the PS composition before completing the stress−strain diagrams.[16] Increasing the weight fraction of the hard segment (PS), the morphology transformed from spheres into lamellas, and accordingly, the elastic modulus and the fracture stress became higher.

By changing temperature (y-axis) instead of changing the composition (x-axis) of triblock copolymers, Khandpur et al. reported a noticeable drop in the measurements of the storage

Received: January 14, 2011
Revised: May 2, 2011
Published: June 15, 2011

Table 1. Annealing Temperatures and the Microphase-Separated Structures

temperature [°C]	microphase-separated structures
175	hexagonally aligned cylindrical phase
200	BCC spherical phase
250	misaligned spherical phase
300	disordered phase

modulus through the transitions from bicontinuous to cylindrical phases examined by linear dynamic mechanical analysis (DMA).[17] Choi et al. detected ODT of spherical microdomains analyzed by plotting the storage modulus G' against the loss modulus G'', again by linear dynamic mechanical analysis.[18] The drop in G' and the change in the slope of G' were generally used to detect a transition temperature in the microstructures.[19,20]

In this study, we studied Vector 4111, a SIS with 18.3 wt % of PS, which is known to possess several OOTs and ODT as described in Figure 1, where the ordered phases change from cylindrical, through BCC spherical, to lattice disordering spherical structures by changing annealing temperatures.[21−23] The relationship between the morphology and the mechanical properties of Vector 4111 through OOT and ODT was extensively studied to understand the linear as well as nonlinear mechanical properties of the triblock copolymer. In particular, G', G'', Young's modulus, fracture stress, fracture strain, and the time−temperature superposition were examined by DMA and by tensile testing. The study would provide a comprehensive explanation on the relationship between the microstructures and the mechanical properties of triblock copolymers through OOT and ODT that can be controlled by temperature, hence industrially readily processable.

EXPERIMENTAL METHODS

Material. The material used in this study is a SIS triblock copolymer (Vector 4111, Dexco Polymers Co.) which has a weight-averaged molecular weight (M_w) of 1.4×10^5 g/mol, with a weight fraction of PS blocks of 0.183, and a polydispersity index (M_w/M_n or PDI) of 1.11. The rubbery feature of the triblock copolymer was due to the physical cross-linkings of the hard PS domains aligned in nanoscale (~1.5 GPa in Young's modulus) with the chemically bonded elastic PI networks (~80 Pa in shear modulus) forming the major parts of the materials. The triblock copolymer was microphase-separated to construct a microphase separated structure that can be considered as an ideal nanocomposite with the interface between PI and PS strongly chemically bonded to form an elastic pseudo-cross-linked material. The viscoelastic moduli of PS and PI are presented in Figure S1 of the Supporting Information. The microphase separation of Vector 4111 has already been studied, and the microstructures were reported to transform with changing annealing temperatures.[9] A hexagonally aligned cylindrical phase was formed below the OOT temperature (T_{OOT}) of 185 °C, and the spherical phase adopting a body-centered cubic (BCC) arrangement was observed between 185 and 215 °C. The BCC lattice was distorted above the lattice disordering transition (LDT) temperature (T_{LDT}) of 215 °C to transform into a misaligned spherical phase below 280 °C. The spherical microdomains finally disappeared to transform into the disordered phase of thermal fluctuations in a single-phase state above the ODT temperature (T_{ODT}) of 280 °C.

Specimen Preparation for Different Morphologies. Vector 4111 pellets sandwiched by two stainless-steel plates covered with polytetrafluoroethylene (PTFE) films were molded under the pressure of 2 MPa. Molding temperatures were set at 175 °C for hex cylinders, 200 °C for BCC spheres, 250 °C for misaligned spheres, and 300 °C for completely disordered state according to the thermal phase properties. Soon after molding, the specimens were quenched using liquid nitrogen, kept for 15 min at very low temperature (−196 °C) in order to fix the microstructures formed at the several annealing temperatures. The thin film substrates were then cut into a 20 × 20 mm square film, and the small-angle X-ray scattering (SAXS) measurements were conducted using the X-ray diffraction equipment (D8 discover, Bruker) to confirm the microphase-separated structures on each sample annealed at different temperatures. The X-ray apparatus consisted of the X-ray generator with Cu Kα radiation using a wavelength of 0.154 nm. The slit width was 0.1 mm with the diameter of a collimator of 0.1 mm. SAXS profiles were measured with the X-ray tube voltage and the current at 40 kV and 40 mA at room temperature. The exposure time to the incident X-ray beam was set at 600 s. The morphology of Vector 4111 was determined by analyzing the relationship between the scattering intensity and the scattering vector q from 0 to 1 nm^{-1}.

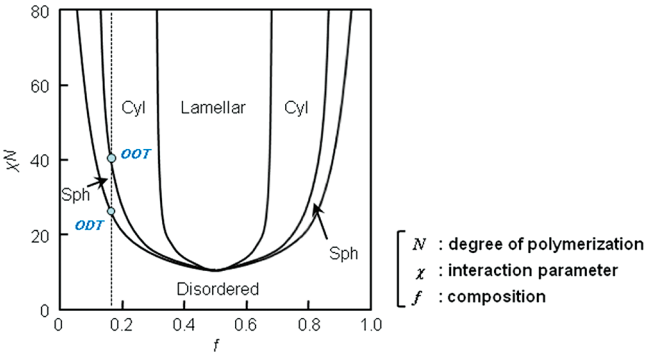

Figure 1. A simplified phase diagram: microphase-separated structure depends on the composition f, segment−segment interaction energy χ, and degree of polymerization N. The dotted line shows $f = 0.183$, where our experiments were carried out with the PS fraction of 0.183 in Vector 4111. The OOT and ODT may be detected at the points described on the dotted line.

AFM observation (SPM, Shimadzu) was carried out to confirm the morphologies during ordering and disordering processes. Vector 4111 was first dissolved into toluene to get 3.23 wt % solutions, and 50 μL of the solution was spin-coated on a silicon substrate. The spin-coated film was then annealed for 12 h in a vacuum oven at several temperatures to form the morphologies shown in Table 1 before the AFM observation by tapping mode.

Phase Transition Temperatures. In order to determine the glass transition temperature (T_g) of the PS component with OOT and ODT temperatures in Vector 4111, dynamic viscoelastic measurements (RSA3 and ARES-G2, TA Instruments) were conducted by changing temperatures. The temperature scanning rate was set at 10 °C/min, and the frequency was set constant at 1.0 Hz. The shear-sandwich geometry was used for the temperature range between 30 and 155 °C, while the oscillation frequency mode with a stainless-steel-serrated parallel plate was used for the temperature range between 155 and 290 °C. The transition temperatures were determined by abrupt changes in the dynamic shear modulus G' which can be well associated with the OOT and the ODT.[17,24]

Viscoelastic Properties and the Time−Temperature Superposition. Linear viscoelastic properties for the different types of microphase-separated structures of elastic Vector 4111 were analyzed by dynamic mechanical analysis in tension mode (RSA3, TA Instruments). The specimens with different morphologies were cut into a rectangular shape, where the length and the width were 30 mm and 10 mm, respectively. The preliminary experiment was first conducted to determine the linear viscoelastic region of the samples, where the tensile

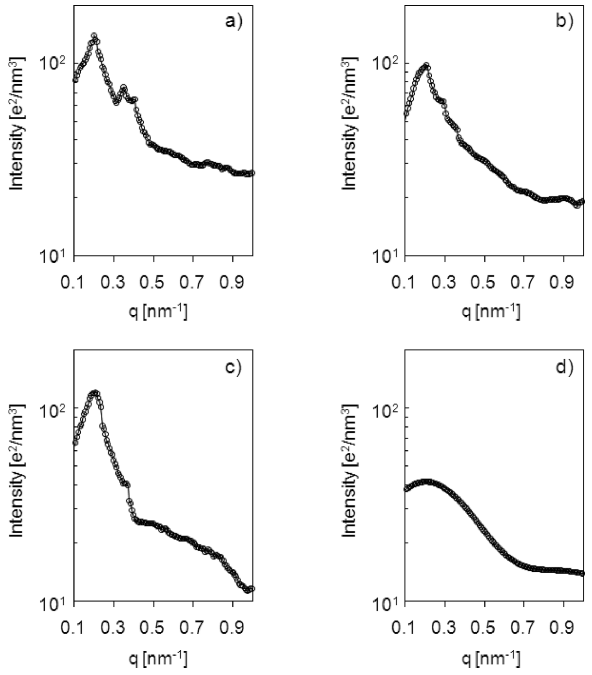

Figure 2. SAXS profiles for the thin film substrate of Vector 4111 at room temperature with the different types of (a) cylindrical, (b) BCC spherical, (c) misaligned spherical, and (d) disordered phases.

storage modulus E', observed by RSA3 in tension mode, remained constant against the change in strain. E' and the tensile loss modulus E'' were measured through dynamic frequency sweep at a strain of 1% by changing frequency from 10 to 0.01 Hz at room temperature (25 °C).

Time−temperature superposition was attempted for each sample followed by the construction of the master curve. For the experiments, dynamic viscoelastic measurements were carried out in shear mode through frequency sweep (RSA3 and ARES-G2, TA Instruments). The sample was measured at the strain of 1.0%, and the frequency was changed from 0.1 to 50 Hz (from 1.0 to 50 Hz in the disordered region). In the cylindrical phase, shear-sandwich geometry was used, while the temperature was changed from 25 to 185 °C. For the samples presenting the BCC arrangement, the misaligned spherical phase, and the disordered region, the oscillation mode controlled by frequency using parallel plates was used at the temperature range between 190 and 300 °C.[9]

Mechanical Properties by Tensile Testing. The mechanical properties of different types of microphase-separated structures were analyzed by a universal tester (AG-IS, Shimadzu). The specimens with different morphologies were cut into a dog bone shape of 16 × 3 × 0.3 mm before the mechanical testing at a tension rate of 5 mm/min at room temperature to create stress−strain curves. The elastic recovery test was also conducted at a strain rate of 5 mm/min by changing the strains (1, 5, 10, 15, and 20) to observe the elastic recovery of the specimens at room temperature in different morphologies. The elastic recovery test is a step cycle test: the tests combined a stepwise stretching of the samples with unloading−reloading cycles. In each step, the sample was extended step by step to the defined five strains. Once it reached the aimed strain (loading process), the speed of extension by the tensile testing machine was automatically inverted until a stress of zero was achieved (unloading process). The strain at which the stress of zero was reached was defined as the residual strain, which directly shows the elastic property of the sample. The elastic recovery rate was defined as the ratio of the residual strain to the applied strain. Once the stress reached zero, then the sample was extended further again at the previous constant strain rate until it reached the next targeted strain (reloading process). The step cycle test

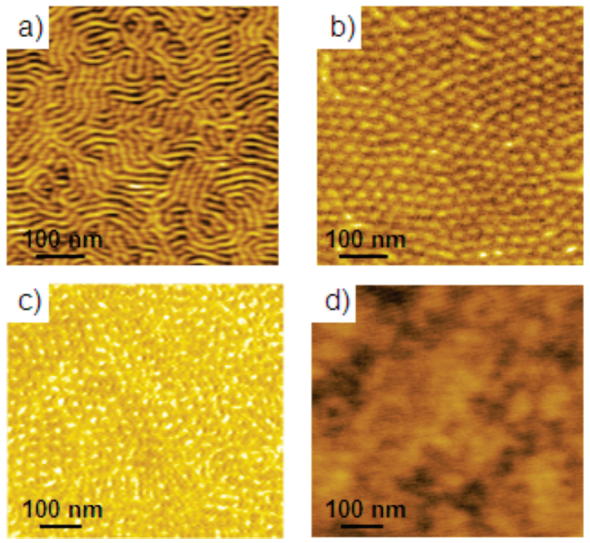

Figure 3. AFM pictures of (a) cylindrical, (b) BCC spherical, (c) misaligned spherical, and (d) disordered phases of Vector 4111.

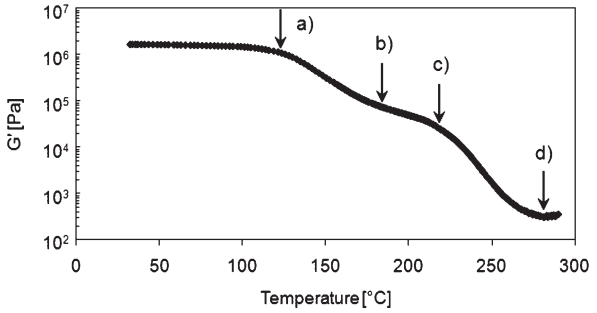

Figure 4. Temperature dependence of the storage elastic modulus: (a) the drop between 115 and 130 °C and the slope changes at (b) 185 °C, (c) 215 °C, and (d) 280 °C, all due to the phase transitions indicated by arrows.

was continuously performed either until the strain reached 20 or up to the point where the sample broke.

It should be noted again that the mechanical experiments for the different types of microphase separation were carried out by using a single Vector 4111.

RESULTS AND DISCUSSION

Structural Analysis by Small-Angle X-ray Scattering. Small-angle X-ray scattering (SAXS) methods were used to investigate the microphase-separated structures of Vector 4111.[25] Figure 2 shows the SAXS profiles of the thin Vector 4111 film which was molded at several temperatures and quenched with liquid nitrogen to form different morphologies listed in Table 1. The X-ray intensity was plotted as a function of the scattering vector q (= $4\pi \sin\theta/\lambda$), with λ and θ being the wavelength of the incident X-ray and the scattering angle, respectively.[3] The profiles had a second-order shoulder or a higher-order peak at $q = \sqrt{3}q_m$ and $\sqrt{4}q_m$ in Figure 2a, at $q = \sqrt{2}q_m$ and $\sqrt{3}q_m$ in Figure 2b, and at $q = \sqrt{3}q_m$ in Figure 2c, where q_m is the first-order peak appearing at $q = 0.2$ nm^{-1}. The intensity peaks disappeared except at $q = q_m$ at the highest temperature (Figure 2d).[26] The results are in good agreement

dx.doi.org/10.1021/ma200087r |Macromolecules 2011, 44, 5310–5317

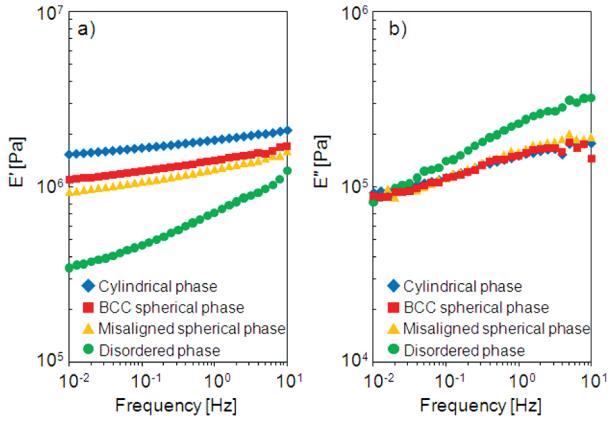

Figure 5. Frequency dependence of (a) the storage and (b) the loss elastic moduli of Vector 4111 at room temperature with the different types of cylindrical, BCC spherical, misaligned spherical, and disordered phases.

with the previous SAXS measurements of SI and SIS block copolymers studied by Hashimoto et al.[27] As for the SAXS profile in Figure 2c, the higher-order shoulder of an intensity peak at $q = \sqrt{3}q_m$ was assigned to a misaligned spherical phase by Hasimoto et al., while in fact, it was found that the peak was caused by the spheres with short-range liquid order, investigated by Percus−Yevick theory on "hard spheres" or by the paracrystal theory.[28] It was therefore concluded that our samples molded at several temperatures based on Table 1 certainly consisted of cylindrical, BCC spherical, misaligned spherical, and disordered phases, and the thin film substrates of Vector 4111 with different morphologies controlled by molding temperatures were successfully obtained.

Observation of Microphase-Separated Structures by AFM. The temperature dependence of the microphase separation was also confirmed by AFM. As shown in Figure 3, the morphology of Vector 4111 was clearly revealed by AFM: Figure 3a shows the cylindrically ordered phase of PS,[3] Figure 3b shows PS spheres packed in a BCC lattice with the [111] projection, Figure 3c shows the spheres packed randomly in the PI matrix,[9] and Figure 3d shows the disordered phase where polymers flow as polymer melt.[29] From these results, it was confirmed that the morphology of Vector 4111 was indeed controlled by annealing temperatures, which remained unchanged once the samples reached the equilibrium state.[30]

Microphase Transition Temperatures Studied by Dynamic Mechanical Analysis. The temperature scans of Vector 4111 by dynamic viscoelastic measurements were carried out to determine the T_g of the PS component and the transition temperatures of the triblock microstructures. Figure 4 shows the temperature dependence of the storage modulus G'. In the temperature range between 115 and 130 °C, a noticeable drop in G' was observed, which corresponded to the T_g of the PS component in Vector 4111. Several other points where the slopes of G' changed were also detected at 185, 215, and 280 °C. These temperatures were considered to be the transition temperatures caused by the changes in the microphase separations of the triblock copolymer, where the transition from cylindrical to BCC spherical phases happened at 185 °C, the transition from BCC spherical to misaligned spherical phases at 215 °C, and finally the disordering phase appeared at 280 °C. It is assumed that during heating the initially ordered phases transfer

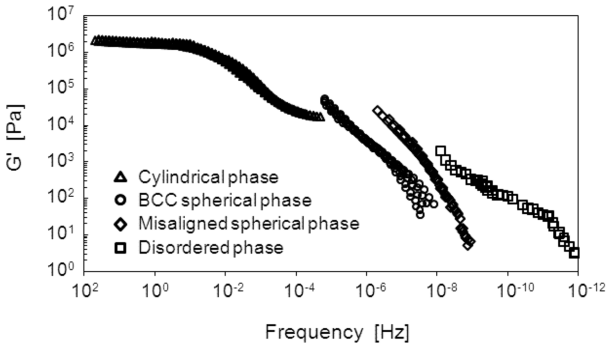

Figure 6. Master curve of Vector 4111 through the order−order and the order−disorder transitions.

to lattice disordered phase and then convert to completely disordered phase followed by the short-range-ordered thermal fluctuation.[31] The results of the dynamic mechanical analysis reflect the molecular interactions between the morphologies of the cylindrical, the BCC spherical, the misaligned spherical, and the disordered phases.[32]

Viscoelastic Behavior in Different Morphologies. In order to analyze the viscoelastic behavior caused by the different morphologies, the frequency dependence of E' and E'' was examined. Figure 5 shows the results of E' and E'' of different morphologies against frequency. According to Figure 5a, it was found that E' was highest in the SIS with the hexagonally cylindrical phase, where E' decreased in the order of the cylindrical, the BCC spherical, the misaligned spherical, and the disordered phases, strongly dependent on the morphology. E'', on the other hand, was highest in the disordered sample. E'' decreased in the samples with the cylindrical, BCC spherical, and the misaligned spherical phases, revealing that the loss energy, i.e., viscous property, was less dominant in the samples of these three morphologies. The noticeable increase in E'' in the disordered sample was highly due to the most liquidlike feature of the polymer melt in the disordered phase. The other three samples with different morphologies exhibited almost the same degree of E'', revealing that the viscous property, in contrast to the elastic property, was almost independent of the ordered phases. The elastic free energy F of elastomers and rubbers can be generally given by

$$F \sim NkT\lambda_k^2$$

where N is the number of cross-linked chains, kT is the thermal energy, and λ_k is the deformation ratios.[33] Considering the elasticity expressed by the chain model, it simply shows that the cross-link density has much effect on the elasticity. The cross-link density n can be expressed by the following form with the elastic modulus E' by Nielsen's empirical equation

$$n = \frac{E\prime}{3RT}$$

where R is the gas constant and T is the absolute temperature.[34,35] The cross-link density is proportional to E', revealed by this equation, so the morphology-dependent cross-link density in our experiments could be considered to decrease in the order of the cylindrical, the BCC spherical, the misaligned spherical, and the disordered phases according to the experimental results of E'. The physical cross-links of the hard PS blocks act for the elastic feature of Vector 4111 with the PI elastic networks; thus, the

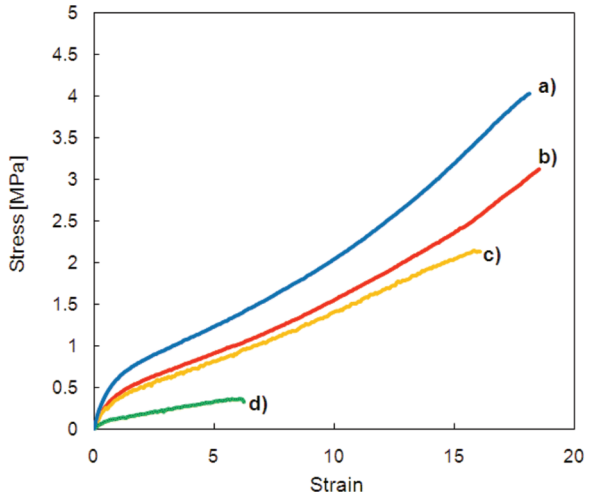

Figure 7. Stress−strain curves of Vector 4111 at room temperature with the different types of (a) cylindrical, (b) BCC spherical, (c) misaligned spherical, and (d) disordered phases.

cylindrical structures of PS worked more as the physical cross-links than the spherical structures, which can be readily understandable from the structural point of view.

Time−Temperature Superposition and the Master Curve. The time−temperature superposition has been extensively examined to obtain the master curve by shifting the values of G' along the time axis. Master curves were almost successfully obtained within each region of the microphase-separated structures except for the BCC region where a slight deviation at the end of the relaxation could be observed as presented in Figure 6. The overall superposition of G' failed to establish a single master curve throughout the order−order and the order−disorder transition temperatures. It was reported that the time−temperature superposition was inefficient and inappropriate to correlate the dynamic viscoelastic properties of triblock copolymers such as SIS and SBS, and diblock copolymers such as SI and SB, over the range of temperatures where thermally induced order−disorder transitions took place.[36] From our experiments, it was found that the relaxation curves of the elastic moduli were almost successfully superposed within each region of the cylindrical, the BCC spherical, the misaligned spherical, and the disordered phases. The slight deviation observed in the tail of the relaxation curves detected in the BCC spherical phase may be due to the partial onset of the misalignment of the spheres, which would be completed up to the temperature of 215 °C. Thus, the BCC spherical structures may have phase-changed to misaligned spherical structures rather than phase transition by temperature. The time−temperature superposition was found to be effective only within the same microphase-separated structures caused by phase transition.

Our results indicate that the relaxation curves of the elastic moduli were almost successfully superposed within each region, where the failures of time−temperature superposition revealed the structural transitions of the microstructures. In more detail, the cylindrical phase, due to the strong incompatibility between the block domains, a relatively long-range orientation existed which totally disappeared above ODT. During such a completely incompatible phase of the cylindrically aligned structures, the time−temperature superposition was successfully applied. In the case of the spherical domains at higher temperature, however, it had been already reported that the long-range order gradually disappeared, which induced a phase change from BCC spherical domains to LDT spherical domains. During such a rather weakly microphase-separated region, the time−temperature superposition could not be entirely applied, where there was a slight deviation observed at the tail of the relaxation curves. It implies that the time−temperature superposition did not work at rather high temperature of the spherical region, where the phase change from BCC to LDT spherical domains occurred. The onset temperature of the failure of the time−temperature superposition, therefore, can be effectively regarded as the LDT temperature, and the further extended failure of the time−temperature superposition above the LDT temperature can be considered as the ODT temperature. In other words, it could be well observed from the time−temperature superposition that during heating the initially ordered phases transferred to lattice disordered phase, followed by the conversion to completely disordered phase with short-range-ordered thermal fluctuation.[31]

Tensile Testing and Elastic Recovery Testing. The results of the stress−strain measurements for Vector 4111 with different morphologies are shown in Figure 7. It was found that the tensile properties varied with different morphologies, although an identical polymer with the same molecular weight and the same molecular composition was used. There have been several reports on the stress−strain behavior of SIS with varying amounts of the hard segment PS (i.e., PS with different molecular weights and with different molecular compositions), where it was concluded that the morphology depended on the weight fraction of PS.[16,37] In their reports, the Young's modulus and the fracture stress became higher with the increase in the molecular weight of PS. Considering our experimental results, it was found that the tensile toughness depended not only on the amount of the hard segment PS but also on the very morphology of the triblock copolymer (i.e., the microphase-separated structures that the triblock copolymer could possess).

From Figure 7, the Young's modulus and the fracture stress increased in the order of the disordered, the misaligned spherical, the BCC spherical, and the cylindrical phases: the Young's moduli were 0.237, 0.646, 0.726, and 1.119 MPa, respectively, and the fracture stresses were 0.624, 2.125, 3.126, and 4.034 MPa, respectively. A recent report by Mclean and Sauer has demonstrated the effect of the tensile strain on the topology of the hard component of a multiblock copolymer. They proposed that the deformation process initiated with the hard component oriented and fractured in their copolymer system, followed by the final mechanical response from the rubber elasticity owing to the soft component.[38] Applying our experimental results to their hypothesis, this morphology−mechanical property relationship can be explored by considering the influence of the structural balance between the hard segment PS and the soft segment PI. Regarding the PS cylindrical phase, deformed PS cylinders caused by mechanical extension could generate separated domains behaving as "quasi-spheres", which could enhance the structural contribution of the soft PI segments due to the lack of continuity of the hard segments that consisted of PS-chain aggregations.[32] This phenomenon could be attributed to the micronecking followed by the breaking of the PS cylindrical domains.[39] The Young's modulus and the fracture stress of the cylindrical sample were therefore higher than those of the spherical samples. It was reported that each cylindrical phase transformed into a column of quasi-spheres in the bicontinuous $Im3m$ phase (the cubic phase of the space group $Im3m$).[40] There the cylindrical phase first

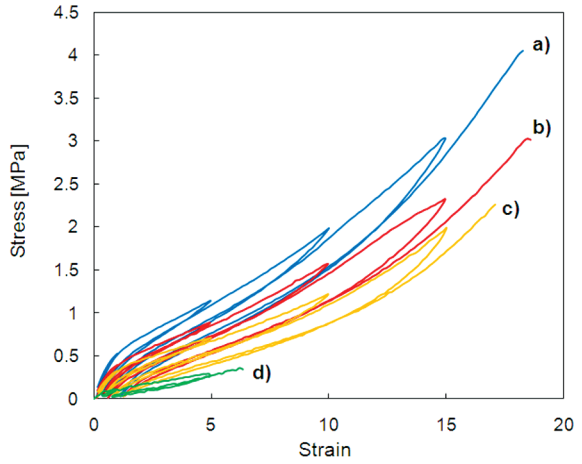

Figure 8. Stress−strain curves of Vector 4111 at room temperature with loading and unloading cycles at strains of 1, 5, 10, and 15 for the different types of (a) cylindrical, (b) BCC spherical, (c) misaligned spherical, and (d) disordered phases.

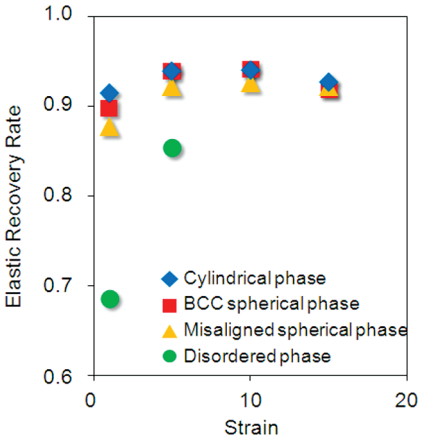

Figure 9. Elastic recovery rate as a function of strain at room temperature for the different types of cylindrical, BCC spherical, misaligned spherical, and disordered phases.

constructed rich networks of hard segments, and then the cylinders started to undulate as if the cylinders were being pinched at regular intervals. The pinch process continued until the narrowest points along the rods were closed off to form discrete spheres. Eventually, the spherical phase possessed more space of soft segments, which resulted in the reduction in the Young's modulus and the fracture stress. As for the BCC and the misaligned spherical phases, a previous study pointed out that elastomers with dispersed sphere particles, whether regularly or randomly aligned, showed little difference in mechanical properties,[41] while other studies reported that the elastic modulus became higher when the spheres were regularly spaced rather than randomly located.[42,43] The latter result was more consistent with our experimental results, where both the Young's modulus and the fracture stress of the BCC spherical phase were higher than those of the misaligned spherical phase. Additionally, in terms of the bridge fractions between PS spherical domains, it is clear that the BCC spherical phase had higher bridge ratio than the misaligned phase, which was also applied to the elastic modulus.[44] For the samples in randomly located spherical phases, hence, the partially long distance between PS spherical domains brought about somewhat spacious microregions, where stress absorption efficiently took place to decrease the elastic modulus. Finally, as for the disordered phase, the structural contribution of the soft segment reached a climax due to the actual loss of the ordered phase of the hard segments. In fact, the soft segments could form continuous phase in matrix, showing maximum softness among all other ordered or disordered samples.

Figure 8 shows the stress−strain curves of the loading and unloading cycles of Vector 4111 with different morphologies to examine the elastic recovery. The same tensile mechanical properties were observed as was observed in Figure 7. Recently, the cylinder morphology has been well studied in terms of the mechanical properties.[45] In this work, it was revealed that the mechanical properties differed with the morphology, showing different loading and unloading mechanical features. Each loading step made an independent contribution to the final deformation, so that the total deformation could be obtained by adding every contribution, which is supported by the principle of the Boltzmann superposition.[46]

From Figure 8, it was found that the ongoing loading never traced the previous loading curves, where the same thing applied to the unloading processes. The second or later loading cycle exhibited a more rubbery character with a significantly lower initial modulus than the previous loading cycle. These stress softening effects with the stress-induced plastic-to-rubber transition of the mechanical properties on the elastomeric triblock copolymer have been well described by Fujimura et al.[47] Figure 9 shows the elastic recovery rate against the applied strain, presenting different elastic recovery features in different morphology. The sample in the disordered phase was ruptured at the strain of 5, while other samples of the three different morphologies exhibited higher elastic recovery rates than 0.9 at strain 15. The initial elastic recovery rates at strain 1 were altogether different from sample to sample, while at higher strains (>5) the trend in the elastic recovery rates became very similar among the samples except for the disordered one. It suggests that the elastic recovery rate examined at larger deformation was almost independent of the morphology of Vector 4111. The elastic recovery rates at lower strain, however, would be vitally affected by the difference in the microphase-separated structures. For example, the remaining cylindrical structures should still be observed at lower strain, but at higher strains, as mentioned in the previous section, the cylindrical phase would transform into quasi-spherical phase due to the rupture of the cylinders, where almost the same elastic recovery rate could be expected in the cylindrical as well as in the spherical phases. At higher strains, the elastic recovery rate became relatively high, where the morphology of PS cylinders and PS spheres was distorted or even broken by the mechanical deformation. The elastic area consisting of PI therefore had a profound impact on the mechanical properties of Vector 4111, where PI phase in the SIS matrix should primarily show the distinctive mechanical characteristics of rubber.

CONCLUSIONS

The mechanical properties of a triblock copolymer possessing different morphology formed at different annealing temperatures were studied. The morphology−mechanical property relationship of the triblock copolymers with different microphase-separated structures was analyzed. The microstructures were confirmed by SAXS measurement. AFM images were obtained to confirm the morphology of the cylindrical, the BCC spherical,

the misaligned spherical, and the disordered phases in differently annealed Vector 4111. The transition temperatures were determined to confirm the validity of the temperatures selected for annealing by observing the dynamic mechanical response of Vector 4111 in tension mode.

Viscoelasticity of the Vector 4111 with different morphology was investigated. It was found that E' decreased in the order of the cylindrical, the BCC spherical, the misaligned spherical, and the disordered phases, strongly dependent on the morphology. Moreover, the time−temperature superposition was attempted and found to be valid only within the same microphase-separated regions or within the disordered phase as shown in Figure 6. However, a slight deviation was observed in the BCC phase at low frequency, which was predominantly due to LDT.

The stress−strain measurements of the triblock copolymer were carried out. The Young's modulus and the fracture stress decreased in the order of the cylindrical, the BCC spherical, the misaligned spherical, and the disordered phases, revealing a strong morphology−mechanical property relationship. It was found that the structural transitions observed in the morphology of Vector 4111 made a significant impact on the mechanical characteristics through the ordering of PS blocks acting as physical cross-links in the PI elastic networks.

■ ASSOCIATED CONTENT

Supporting Information. Viscoelastic moduli of both PI and PS. This material is available free of charge via the Internet at http://pubs.acs.org.

■ AUTHOR INFORMATION

Corresponding Author

*Tel +81-45-566-1604; Fax +81-45-566-1495; e-mail hotta@mech.keio.ac.jp.

■ ACKNOWLEDGMENT

This work was supported in part by a Grant-in-Aid for the Global Center of Excellence Program for the "Center for Education and Research of Symbiotic, Safe and Secure System Design" from the Ministry of Education, Culture, Sport, and Technology in Japan (A.H.), a Grant-in-Aid for Scientific Research (B) from the Japan Society for the Promotion of Science (JSPS: "KAKENHI") (No. 23360294 to A.H.), a Grant-in-Aid for Scientific Research (S) (No. 21226006 to A.H.), and a Grant-in-Aid for Scientific Research on Innovative Areas (No. 22110-516 to A.H.).

■ REFERENCES

(1) Hafner, O. T.; Goritz, D. *Kautschuk Gummi Kunststoffe* **1995**, *48* (11), 778.
(2) Pixa, R.; Schirrer, R. *Colloid Polym. Sci.* **1981**, *259* (4), 435–446.
(3) Sota, N.; Sakamoto, N.; Saijo, K.; Hashimoto, T. *Macromolecules* **2003**, *36* (12), 4534–4543.
(4) Yokoyama, H. *Mater. Sci. Eng., R* **2006**, *53* (5−6), 199–248.
(5) Rodríguez-Hidalgo, M.-d.-R.; Soto-Figueroa, C.; Martínez-Magadán, M.; Luís-Vicente *Polymer* **2009**, *50* (19), 4596–4601.
(6) Lee, W. K.; Lim, H.; Kim, E. Y. *J. Nanosci. Nanotechnol.* **2008**, *8* (9), 4771–4774.
(7) Qiao, B. F.; Zhao, D. L. *J. Chem. Phys.* **2004**, *121* (10), 4968–4973.
(8) Taylor, P. L.; Yu, Y. K.; Wang, X. Y. *J. Chem. Phys.* **1996**, *105* (3), 1237–1241.
(9) Sakamoto, N.; Hashimoto, T. *Macromolecules* **1998**, *31* (24), 8493–8502.
(10) Kim, M. I.; Wakada, T.; Akasaka, S.; Nishitsuji, S.; Saijo, K.; Hasegawa, H.; Ito, K.; Takenaka, M. *Macromolecules* **2008**, *41* (20), 7667–7670.
(11) Miao, B.; Wickham, R. A. *J. Chem. Phys.* **2008**, *128* (5), xxxx.
(12) He, G. L.; Merlitz, H.; Sommer, J. U.; Wu, C. X. *Macromolecules* **2009**, *42* (18), 7194–7202.
(13) Qin, Q.; Shi, X. F.; McKenna, G. B. *J. Polym. Sci., Part B: Polym. Phys.* **2007**, *45* (24), 3277–3284.
(14) Leibler, L. *Macromolecules* **1980**, *13* (6), 1602–1617.
(15) Floudas, G.; Pispas, S.; Hadjichristidis, N.; Pakula, T.; Erukhimovich, I. *Macromolecules* **1996**, *29* (11), 4142–4154.
(16) Honeker, C. C.; Thomas, E. L. *Chem. Mater.* **1996**, *8* (8), 1702–1714.
(17) Khandpur, A. K.; Forster, S.; Bates, F. S.; Hamley, I. W.; Ryan, A. J.; Bras, W.; Almdal, K.; Mortensen, K. *Macromolecules* **1995**, *28* (26), 8796–8806.
(18) Choi, S.; Lee, K. M.; Han, C. D.; Sota, N.; Hashimoto, T. *Macromolecules* **2003**, *36* (3), 793–803.
(19) Rubinstein, M.; Obukhov, S. P. *Macromolecules* **1993**, *26* (7), 1740–1750.
(20) Rosedale, J. H.; Bates, F. S. *Macromolecules* **1990**, *23* (8), 2329–2338.
(21) Krishnamoorti, R.; Modi, M. A.; Tse, M. F.; Wang, H. C. *Macromolecules* **2000**, *33* (10), 3810–3817.
(22) Shin, C.; Ryu, D. Y.; Huh, J.; Kim, J. H.; Kim, K. W. *Macromolecules* **2009**, *42* (6), 2157–2160.
(23) Widmaier, J. M.; Meyer, G. C. *J. Therm. Anal.* **1982**, *23* (1−2), 193–199.
(24) Forster, S.; Khandpur, A. K.; Zhao, J.; Bates, F. S.; Hamley, I. W.; Ryan, A. J.; Bras, W. *Macromolecules* **1994**, *27* (23), 6922–6935.
(25) Suehiro, S.; Saijo, K.; Ohta, Y.; Hashimoto, T.; Kawai, H. *Anal. Chim. Acta* **1986**, *189* (1), 41–56.
(26) Wang, X. H.; Dormidontova, E. E.; Lodge, T. P. *Macromolecules* **2002**, *35* (26), 9687–9697.
(27) Hashimoto, T.; Suehiro, S.; Shibayama, M.; Saijo, K.; Kawai, H. *Polym. J.* **1981**, *13* (5), 501–516.
(28) Han, C. D.; Vaidya, N. Y.; Kim, D.; Shin, G.; Yamaguchi, D.; Hashimoto, T. *Macromolecules* **2000**, *33* (10), 3767–3780.
(29) Sakamoto, N.; Hashimoto, T. *Macromolecules* **1998**, *31* (10), 3292–3302.
(30) Sakamoto, N.; Hashimoto, T.; Han, C. D.; Kim, D.; Vaidya, N. Y. *Macromolecules* **1997**, *30* (6), 1621–1632.
(31) Ahn, D. U.; Sancaktar, E. *Int. J. Mol. Sci.* **2009**, *10* (5), 2169–2189.
(32) Ryu, C. Y.; Lodge, T. P. *Macromolecules* **1999**, *32* (21), 7190–7201.
(33) Vilgis, T. A.; Heinrich, G. *Angew. Makromol. Chem.* **1992**, *202*, 243–259.
(34) Nielsen, L. E. *J. Appl. Polym. Sci.* **1964**, *8*, 511–520.
(35) Nielsen, L. E.; Landel, R. F. *Mechanical Properties of Polymers and Composites*; Marcel Dekker Inc.: New York, 1994; p 168.
(36) Han, C. D.; Kim, J. *J. Polym. Sci., Part B: Polym. Phys.* **1987**, *25* (8), 1741–1764.
(37) Dair, B. J.; Honeker, C. C.; Alward, D. B.; Avgeropoulos, A.; Hadjichristidis, N.; Fetters, L. J.; Capel, M.; Thomas, E. L. *Macromolecules* **1999**, *32* (24), 8145–8152.
(38) McLean, R. S.; Sauer, B. B. *J. Polym. Sci., Part B: Polym. Phys.* **1999**, *37* (8), 859–866.
(39) Stasiak, J.; Squires, A. M.; Castelletto, V.; Hamley, I. W.; Moggridge, G. D. *Macromolecules* **2009**, *42* (14), 5256–5265.
(40) Sakya, P.; Seddon, J. M.; Templer, R. H.; Mirkin, R. J.; Tiddy, G. J. T. *Langmuir* **1997**, *13* (14), 3706–3714.
(41) Pu, Z. C.; Mark, J. E.; Jethmalani, J. M.; Ford, W. T. *Chem. Mater.* **1997**, *9* (11), 2442–2447.

(42) Mark, J. E.; Abou-Hussein, R.; Sen, T. Z.; Kloczkowski, A. *Polymer* **2005**, *46* (21), 8894–8904.
(43) Dair, B. J.; Avgeropoulos, A.; Hadjichristidis, N.; Thomas, E. L. *J. Mater. Sci.* **2000**, *35* (20), 5207–5213.
(44) Takano, A.; Kamaya, I.; Takahashi, Y.; Matsushita, Y. *Macromolecules* **2005**, *38* (23), 9718–9723.
(45) Honeker, C. C.; Thomas, E. L.; Albalak, R. J.; Hajduk, D. A.; Gruner, S. M.; Capel, M. C. *Macromolecules* **2000**, *33* (25), 9395–9406.
(46) Ward, I. M. S. J. *An Introduction to the Mechanical Properties of Solid Polymers*; John Wiley & Sons: New York, 2004; p 59.
(47) Fujimura, M.; Hashimoto, T.; Kawai, H. *Rubber Chem. Technol.* **1978**, *51* (2), 215–224.